Frequency tuning, nonlinearities and mode coupling in circular mechanical graphene resonators

2013 Nanotechnology 24 395702

(http://iopscience.iop.org/0957-4484/24/39/395702)

Nanotechnology **24** (2013) 395702 (9pp) doi:10.1088/0957-4484/24/39/395702

Frequency tuning, nonlinearities and mode coupling in circular mechanical graphene resonators

A M Eriksson, D Midtvedt, A Croy and A Isacsson

Department of Applied Physics, Chalmers University of Technology SE-412 96, Göteborg, Sweden

E-mail: andreas.isacsson@chalmers.se

Received 16 May 2013, in final form 6 August 2013
Published 5 September 2013
Online at stacks.iop.org/Nano/24/395702

Abstract

We study circular nanomechanical graphene resonators by means of continuum elasticity theory, treating them as membranes. We derive dynamic equations for the flexural mode amplitudes. Due to the geometrical nonlinearity the mode dynamics can be modeled by coupled Duffing equations. By solving the Airy stress problem we obtain analytic expressions for the eigenfrequencies and nonlinear coefficients as functions of the radius, suspension height, initial tension, back-gate voltage and elastic constants, which we compare with finite element simulations. Using perturbation theory, we show that it is necessary to include the effects of the non-uniform stress distribution for finite deflections. This correctly reproduces the spectrum and frequency tuning of the resonator, including frequency crossings.

(Some figures may appear in colour only in the online journal)

1. Introduction

In the field of nanoelectromechanical (NEM) systems, nonlinear dynamic phenomena such as bifurcations and mode coupling are receiving increasing interest [1–10]. In particular, graphene resonators [3, 11–18], are known to display strong geometric nonlinear conservative as well as nonlinear dissipative response [2, 13, 14, 19–21]. This opens up for new device applications [24] as well as for fundamental research [25, 26]. So far, however, much of the work on nonlinear dynamics has focused on one-dimensional systems with beam or string like behavior. In graphene resonator devices, the geometries have mostly been rectangular and doubly clamped. Such resonators tend to suffer from inhomogeneous strain and ill defined mode shapes [27] and can possess edge modes or scrolled edges degrading the quality factor [28]. To alleviate these problems, circular graphene drum resonators, which are edge and corner free, can be used [29].

Treating a circular graphene resonator (see figure 1) as a membrane [30], we derive analytic expressions for frequency tuning, Duffing constants and mode coupling coefficients as functions of prestress, radius, electrostatic pressure, and elastic parameters. Knowledge of these coefficients is required when analyzing and designing experiments. The treatment here also applies to other nanomechanical membrane resonators made from for instance SiN or GaAs [22, 23]. However, the extremely strong geometric nonlinearities of graphene resonators make them occupy a particular niche, which is why we focus around these in this work.

The study of the nonlinear dynamics of membranes and thin shells has a long history in the field of applied mechanics and structural engineering. For instance the static deflection solutions corresponding to the Hencky problem [31, 32] and fundamental mode nonlinearity [33], have been studied previously; for a review see [34]. In NEM-resonator experiments, typically only a few flexural resonant modes are excited and probed. The equations of motion for the normal mode coordinates $\zeta_\alpha(\tau)$, which are nonlinear due to the geometric nonlinearity, have the canonical form

$$\partial_\tau^2\zeta_\alpha + \Lambda_\alpha\zeta_\alpha + \sum_{\beta=1}^{\infty}\sum_{\gamma\geq\beta}^{\infty} Q^\alpha_{\beta\gamma}\zeta_\beta\zeta_\gamma + \sum_{\beta=1}^{\infty}\sum_{\gamma\geq\beta}^{\infty}\sum_{\eta\geq\gamma}^{\infty} C^\alpha_{\beta\gamma\eta}\zeta_\beta\zeta_\gamma\zeta_\eta = f_\alpha(\tau). \quad (1)$$

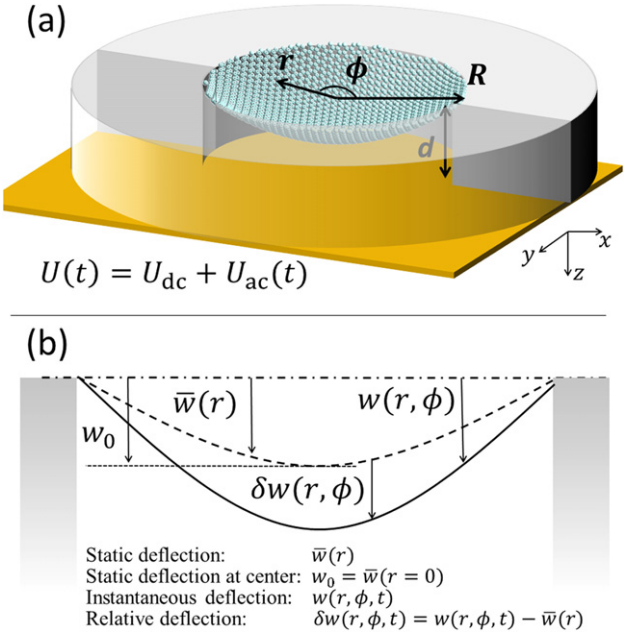

Figure 1. (a) Circular graphene NEM-resonator of radius R. A back-gate located a distance d below the membrane can tune and actuate the resonator by a dc-voltage $U_{\rm dc}$ and a time varying ac-voltage $U_{\rm ac}$, respectively. (b) Introduced notations for vertical deflections. Before bias, the sheet is assumed to be lying flat in the xy-plane (dash-dotted line). The electrostatic pressure from the back-gate introduces a static vertical deformation $\bar{w}(r)$ (dashed line). The maximum static deflection at the center is denoted by w_0. The total instantaneous deflection of the vibrating sheet is denoted by $w(r, \phi, t)$ (solid line).

In this nonlinear Duffing equation $f_\alpha(\tau)$ represents external forcing and Λ_α are the eigenfrequencies squared. This form facilitates the description and analysis of the system dynamics. Using first order perturbation theory, and comparing with finite elements simulations, we give closed expressions for Λ_α and coupling constants $Q^\alpha_{\beta\gamma}$ and $C^\alpha_{\beta\gamma\eta}$. We find that significant contributions to the frequency spectrum come from inclusion of the deflection-induced non-uniform tension. In particular it gives rise to frequency crossings, i.e., an interchange of mode frequencies with increasing back-gate voltage.

The organization of this paper is as follows: first, in section 2, we present and discuss the validity of treating a graphene resonator as a membrane. Then, in section 3, we consider the problem of finding the static shape and accompanying non-uniform tension profile in the presence of a static back-gate voltage. We then, in section 4, reformulate the problem in terms of the coupled Duffing equations (1), while section 5 treats the frequency spectrum of the lowest lying modes as well as the frequency tuning with back-gate voltage. Finally, in section 6 we calculate the quadratic and cubic nonlinear coupling constants appearing in (1).

2. Continuum description of suspended graphene

We consider a circular mechanical resonator of radius R made from a single layer of graphene with a built-in uniform tensile stress T_0 and suspended a distance d above a back-gate, as sketched in figure 1. The external forces on the membrane stem from the gate bias voltage $U(t) = U_{\rm dc} + U_{\rm ac}(t)$. In this work the response of the driving field due to $U_{\rm ac}$ is not studied. Instead, our aim is to derive, as functions of system parameters, the coefficients for the system of nonlinear ordinary differential equations describing the mode dynamics. This connects the graphene resonator dynamics to the vast body of results already present for driven single or coupled nonlinear resonator systems.

The displacement field $\boldsymbol{u}(r, \phi) = u_r(r, \phi)\hat{r} + u_\phi(r, \phi)\hat{\phi} + w(r, \phi)\hat{z}$ describes the local deviation of the graphene from its relaxed and ideally flat configuration when it is free of tension. We assume that for zero static voltage the displacement field $\boldsymbol{u} = 0$, i.e. no intrinsic deformation of the membrane from the manufacturing of the graphene resonators. The equations of motion for the membrane follow from the Lagrangian density $\mathcal{L} = \mathcal{T} - (\mathcal{V}_{\rm b} + \mathcal{V}_{\rm s})$ consisting of kinetic energy density $\mathcal{T}$, bending energy density $\mathcal{V}_{\rm b} = \frac{\kappa}{2}|\Delta w|^2$ and stretching energy density $\mathcal{V}_{\rm s} = \frac{1}{2}\sigma_{ij}\epsilon_{ij}$. Here, κ is the bending rigidity while the stress (σ_{ij}) and strain (ϵ_{ij}) components are

$$\begin{aligned} \sigma_{rr} &= \frac{Eh}{1-\nu^2}\left(\epsilon_{rr} + \nu\epsilon_{\phi\phi}\right), \\ \epsilon_{rr} &= \partial_r u_r + \tfrac{1}{2}(\partial_r w)^2, \end{aligned} \tag{2}$$

$$\begin{aligned} \sigma_{\phi\phi} &= \frac{Eh}{1-\nu^2}\left(\epsilon_{\phi\phi} + \nu\epsilon_{rr}\right), \\ \epsilon_{\phi\phi} &= \frac{1}{r}\partial_\phi u_\phi + \frac{1}{r}u_r + \frac{1}{2r^2}(\partial_\phi w)^2, \end{aligned} \tag{3}$$

$$\begin{aligned} \sigma_{r\phi} &= \frac{Eh}{1+\nu}\epsilon_{r\phi}, \\ \epsilon_{r\phi} &= \frac{1}{2}\left[\left(\partial_r - \frac{1}{r}\right)u_\phi + \frac{1}{r}\partial_\phi u_r + \frac{1}{r}(\partial_r w)(\partial_\phi w)\right]. \end{aligned} \tag{4}$$

For graphene, the elastic modulus E and the mechanical equivalent membrane thickness h are combined in the 2D modulus $Eh \approx 340\ \mathrm{N\,m^{-1}}$ and the Poisson ratio $\nu \approx 0.15$ [35]. These quantities relate to the 2D Lamé coefficients $\lambda = Eh\nu/(1-\nu^2)$ and $\mu = Eh/2(1+\nu)$. Stationarity of the action leads to the Föppl–von Karman equations of motion

$$\rho_0\ddot{u}_r - [\partial_r\sigma_{rr} + r^{-1}\partial_\phi\sigma_{r\phi} + r^{-1}(\sigma_{rr} - \sigma_{\phi\phi})] = 0, \tag{5}$$

$$\rho_0\ddot{u}_\phi - [\partial_r\sigma_{r\phi} + 2r^{-1}\sigma_{r\phi} + r^{-1}\partial_\phi\sigma_{\phi\phi}] = 0, \tag{6}$$

$$\begin{aligned} &\rho_0\ddot{w} + \kappa\Delta^2 w - r^{-1}[\partial_r(r\sigma_{rr}\partial_r w + \sigma_{r\phi}\partial_\phi w) \\ &\quad + \partial_\phi(\sigma_{r\phi}\partial_r w + r^{-1}\sigma_{\phi\phi}\partial_\phi w)] = P_z(r, \phi), \end{aligned} \tag{7}$$

with mass density $\rho_0 \approx 0.75\ \mathrm{mg\ m^{-2}}$ [35] and external load P_z. For an initial uniform strain ϵ_0, the boundary conditions supplementing (5)–(7) are

$$\begin{aligned} \boldsymbol{u}(r, 2\pi) = \boldsymbol{u}(r, 0), \qquad u_r(R, \phi) = R\epsilon_0, \\ u_\phi(R, \phi) = w(R, \phi) = \partial_r w|_{r=R} = 0. \end{aligned} \tag{8}$$

For the electrostatic load, we adopt the local parallel plate approximation, i.e., $P_z(r) = -(U(t)^2/2)\partial_{\tilde{z}}C$, with $\tilde{z}(r, \phi, t) = d - w(r, \phi, t)$ and distance dependent capacitance C. Upon decomposing the vertical deflection into a static and a time

dependent part as $w(r, \phi, t) = \bar{w}(r, \phi) + \delta w(r\phi, t)$, one has to lowest order in δw

$$P_z = \frac{\varepsilon_0 U^2}{2(d-w)^2} \approx \frac{\varepsilon_0 U^2}{2(d-\bar{w})^2}\left(1 + 2\frac{\delta w}{d-\bar{w}}\right), \qquad (9)$$

where ε_0 is the vacuum permittivity.

Before attempting to solve the problem, we can make some considerable simplifications. Since graphene has a very low bending rigidity, $\kappa \approx 1.5$ eV [35, 36], the ratio between bending and stretching terms in (7) is very small for the lowest lying flexural vibration modes, if a built-in tension is present [37]. Hence, we employ the membrane approximation where the bending rigidity is neglected. Further, since the lowest frequencies of in-plane vibrations are typically one or two orders of magnitude larger than the frequencies of the lowest lying out-of-plane vibrations, we can treat the in-plane displacements adiabatically. Hence, we drop the terms $\ddot{u}_r = \ddot{u}_\phi = 0$ in (5) and (6) and solve the ensuing equilibrium equations as functions of w.

To solve the simplified in-plane problem we introduce the Airy stress field χ [38] satisfying the inhomogeneous biharmonic equation

$$\Delta^2 \chi(r, \phi, t) = EhR^{-2} F[w, w], \qquad (10)$$

where the source term $F[w, w]$ is bilinear in its two arguments, and defined by

$$\begin{aligned} 2R^{-2}F[w, w'] = &-(\partial_r^2 w)(r^{-1}\partial_r w' + r^{-2}\partial_\phi^2 w') \\ &- (r^{-1}\partial_r w + r^{-2}\partial_\phi^2 w)(\partial_r^2 w') \\ &+ 2(\partial_r r^{-1}\partial_\phi w)(\partial_r r^{-1}\partial_\phi w'). \end{aligned} \qquad (11)$$

By decomposing the Airy function as $\chi = \sum_n e^{in\phi}\chi_n(r)$ the general inhomogeneous problem on the disk $\Delta^2\chi = F$ can be solved by means of integration (see appendix).

The function χ relates linearly to the stress components as [39]

$$\begin{aligned} \sigma_{rr} &= T_0 + r^{-1}\partial_r\chi + r^{-2}\partial_\phi^2\chi, \\ \sigma_{\phi\phi} &= T_0 + \partial_r^2\chi, \qquad \sigma_{r\phi} = -\partial_r(r^{-1}\partial_\phi\chi). \end{aligned} \qquad (12)$$

The problem is then reduced to solving the nonlinear out-of-plane equation

$$\begin{aligned} &\rho_0\partial_t^2 w - r^{-1}[\sigma_{rr}r\partial_r^2 w + 2\sigma_{r\phi}\partial_\phi(\partial_r - r^{-1})w \\ &+ \sigma_{\phi\phi}(\partial_r + r^{-1}\partial_\phi^2)w] = P_z, \end{aligned} \qquad (13)$$

where we obtain σ_{ij} from solving (10) and using the relations (12).

For convenience we will from here on use dimensionless variables $\tau = tR^{-1}\sqrt{T/\rho_0}$, $\rho = r/R$, $\upsilon_r = u_r/R$, $\upsilon_\phi = u_\phi/R$, $\zeta = w/R$, and $\Phi_z = P_z R/T$, where T is the uniform part of the stress including the stiffening when deflecting the membrane, defined in (19).

In our treatment, the graphene is taken to be flat although graphene devices often show some form of corrugation or rippling. Thermal ripples are known to cause renormalization of the bending rigidity [40]. However, for a clamped membrane under tensile stress this renormalization is too small to be significant for the graphene resonator dynamics [37]. Another source of corrugation is if the built-in tension is not uniform which can lead to wrinkling of the sheet [41]. For a graphene resonator to operate well, tension should be uniform and the sheet void of wrinkles. If wrinkles are present, the simple membrane model used here is not valid, and a more elaborate treatment is needed. Further, grain boundaries will typically be present in graphene made by chemical vapor deposition (CVD). As grain boundaries break the circular symmetry of the resonator, degeneracies will be lifted and introduce corrections to mode coupling constants.

3. Static deformation

To address the dynamics, we must solve the static problem to find the time-independent components of the deformation field which we denote by $(\bar{\upsilon}_r, \bar{\upsilon}_\phi, \bar{\zeta})$. As the load has axial symmetry, $\bar{\upsilon}_\phi \equiv 0$, while $\bar{\upsilon}_r$ and $\bar{\zeta}$ are found from solving (13) with $\partial_t^2 w = 0$. To this end we make the Ansatz $\bar{\zeta}(\rho) = \zeta_0(1-\rho^2)$ where the scaled maximum deflection at the center of the resonator $\zeta_0 = w_0/R$ is the variational parameter. With this Ansatz one finds for the static radial displacement

$$\bar{\upsilon}_r(\rho) = \rho[(T_0/Eh)(1-\nu) + (\zeta_0/4)(3-\nu)(1-\rho^2)], \qquad (14)$$

and that ζ_0 is found from solving a cubic equation. The latter gives

$$\begin{aligned} \zeta_0 &= b(2/3\theta)^{1/3} - (\theta/18c^3)^{1/3}, \\ \theta &= \sqrt{3}\sqrt{4b^3c^3 + 27a^2c^4} - 9ac^2. \end{aligned} \qquad (15)$$

For a uniform load the constants appearing in (15) are $a = -R\varepsilon_0 U_{\mathrm{dc}}^2/4Ehd^2$, $b = 2T_0/Eh$, and $c = (7-\nu)/6(1-\nu)$. If $\bar{\Phi}_z$ is modeled by the local parallel plate approximation, corrections to the constants can be calculated. To lowest order in w_0/d one finds that a and c remain unchanged while $b = 2T_0/Eh + 2R^2\varepsilon_0 U_{\mathrm{dc}}^2/3Ehd^3$.

Equation (15) can be used to calculate the static center deflection $\zeta_0 = w_0/R$ as a function of back-gate voltage U_{dc} for arbitrary values of the radius R, prestress T_0 and suspension height d. The static shape of the membrane then follows from equation (14).

The result from the uniform load approximation is shown in figure 2 where the maximum displacement for the variational Ansatz has been compared to finite element simulations using COMSOL Multiphysics. The values for the prestress T_0 were chosen to conform with experimentally observed values [2, 11]. Note that $T_0 = 0.34$ N m^{-1} corresponds to a built-in strain of the order 0.1%. The agreement between the analytical model and the numerical simulations under uniform load is very good, showing that the Ansatz and disregarding the bending rigidity are valid approximations.

4. Mode expansion and coupled Duffing equations

Having found the expression for the static solution we turn to the problem of setting up the equations for small vibrations around equilibrium. Expressing these as $\delta\zeta = \zeta - \bar{\zeta}$, the

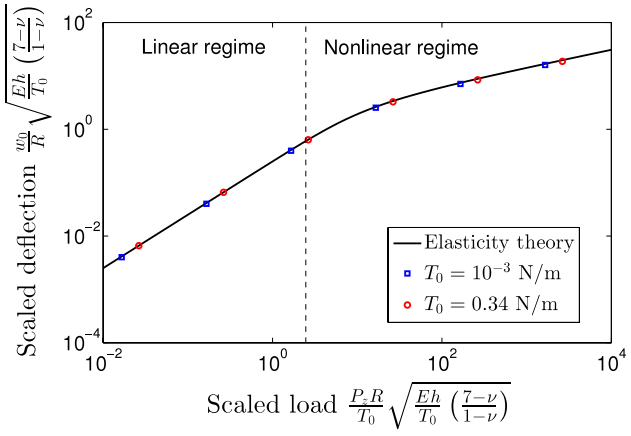

Figure 2. Comparison of the analytical model and numerical simulations of the static vertical deflection at the center of the membrane $w_0 = w(r = 0)$, due to a uniform electrostatic pressure P_z. Symbols result from COMSOL Multiphysics simulations with low (blue squares) and high (red circles) uniform prestress T_0. The solid line corresponds to the solution obtained from the variational Ansatz $w(r) = w_0(1 - [r/R]^2)$ for the vertical deflection and neglecting bending rigidity. For small loads the deflection is linear in P_z and then crosses over to a nonlinear regime where $w_0 \propto P_z^{1/3}$ [39].

system of differential equations for the out-of-plane deflection (see (10) and (13)) can be formally stated as

$$\partial_\tau^2 \delta\zeta - [\hat{L} + \hat{K}]\delta\zeta = \delta\Phi_z. \tag{16}$$

Here $\delta\Phi_z$ is the time dependent part of the external force, $\hat{L}$ is a linear operator and $\hat{K}$ an operator corresponding to the nonlinear part of the problem. Both operators depend on the static deflection $\bar{\zeta}$.

To obtain equations for the mode amplitudes, we expand the vertical displacement in eigenmodes of the eigenvalue problem $\hat{L}\Psi_\alpha + \Lambda_\alpha\Psi_\alpha = 0$ as

$$\zeta(\rho, \phi, \tau) = \bar{\zeta}(\rho) + \sum_\alpha \zeta_\alpha(\tau)\Psi_\alpha(\rho, \phi). \tag{17}$$

The composite mode index $\alpha = (n_\alpha, k_\alpha)$ consists of an angular component n_α and a radial component k_α, such that $\Psi_\alpha(\rho, \phi) = \mathrm{e}^{\mathrm{i}n_\alpha\phi}\Psi_{n_\alpha,k_\alpha}(\rho)$.

To obtain the coefficients in equation (1) it is useful to first consider the stress fields. As the stresses in (12) are linear in χ which, in turn, is bilinear in the arguments of F (see (11)), also the stresses will be bilinear in the arguments of F. Hence, using bilinearity we can decompose the stress fields corresponding to a displacement $\zeta = \bar{\zeta} + \delta\zeta$ into a static part and time dependent linear and nonlinear parts in $\delta\zeta$, i.e.,

$$\sigma_{ij}[\zeta, \zeta] = T[\bar{\zeta}, \bar{\zeta}] + \bar{\sigma}_{ij}[\bar{\zeta}, \bar{\zeta}] + 2\sum_\alpha \zeta_\alpha\sigma_{ij}[\bar{\zeta}, \Psi_\alpha] + \sum_{\alpha\beta}\zeta_\alpha\zeta_\beta\sigma_{ij}[\Psi_\alpha, \Psi_\beta]. \tag{18}$$

The notation $\sigma_{ij}[f, g]$ indicates that this stress is found from solving $\Delta^2\chi = EhR^{-2}F[f, g]$. We have further divided the static stress into one uniform part T and one spatially dependent part $\bar{\sigma}_{ij}$. Explicit calculations show that

$$\begin{aligned} T &= T_0(1 + x^2/4), \\ x &= \zeta_0(Eh/T_0)^{1/2}\sqrt{(3-\nu)/(1-\nu)}, \end{aligned} \tag{19}$$

with the scaled static center deflection x.

The coupled mode equations are obtained from inserting the expansion (17) in the out-of-plane equation (13) along with the expansion (18) and projecting it onto each eigenmode Ψ_α. This leads to the desired system of nonlinear coupled Duffing equations

$$\partial_\tau^2\zeta_\alpha + \Lambda_\alpha\zeta_\alpha + \sum_{\beta=1}^{\infty}\sum_{\gamma\geq\beta}^{\infty} Q^\alpha_{\beta\gamma}\zeta_\beta\zeta_\gamma + \sum_{\beta=1}^{\infty}\sum_{\gamma\geq\beta}^{\infty}\sum_{\eta\geq\gamma}^{\infty} C^\alpha_{\beta\gamma\eta}\zeta_\beta\zeta_\gamma\zeta_\eta = \langle\Psi_\alpha^*\delta\Phi_z\rangle. \tag{20}$$

Here, $\langle\Psi_\alpha^*\Psi_\beta\rangle = \int_0^{2\pi}\int_0^1 \mathrm{d}\phi\,\mathrm{d}\rho\ \rho\Psi_\alpha^*\Psi_\beta$, where * denotes complex conjugation. We can now identify the linear operator in (16) as $L = \nabla^2 + \hat{V}$ with

$$\hat{V}\delta\zeta = T^{-1}\left(\bar{\sigma}_{rr}\partial_\rho^2\delta\zeta + \bar{\sigma}_{\phi\phi}\left(\rho^{-1}\partial_\rho + \rho^{-2}\partial_\phi^2\right)\delta\zeta + 2\sigma_{rr}[\bar{\zeta}, \delta\zeta]\partial_\rho^2\bar{\zeta} + 2\sigma_{\phi\phi}[\bar{\zeta}, \delta\zeta]\rho^{-1}\partial_\rho\bar{\zeta}\right). \tag{21}$$

The overlaps with the nonlinear operator $\hat{K}$ give rise to the double sum containing the constants $Q^\alpha_{\beta\gamma}$ and the triple sum containing the constants $C^\alpha_{\beta\gamma\eta}$. The quadratic coupling constants are defined by

$$\begin{aligned} Q^\alpha_{\beta\gamma} = -T^{-1}\Big\langle &\Psi_\alpha^*[2\sigma_{rr}[\bar{\zeta}, \Psi_\beta]\partial_\rho^2\Psi_\gamma \\ &+ 4\mathrm{i}n_\gamma\sigma_{r\phi}[\bar{\zeta}, \Psi_\beta]\partial_\rho(\rho^{-1}\Psi_\gamma) + \sigma_{rr}[\Psi_\beta, \Psi_\gamma]\partial_\rho^2\bar{\zeta} \\ &+ 2\sigma_{\phi\phi}[\bar{\zeta}, \Psi_\beta](\rho^{-1}\partial_\rho - n_\gamma^2\rho^{-2})\Psi_\gamma \\ &+ \sigma_{\phi\phi}[\Psi_\beta, \Psi_\gamma]\rho^{-1}\partial_\rho\bar{\zeta}]\Big\rangle_{\beta\gamma}, \end{aligned} \tag{22}$$

where the subscripts on $\langle\cdots\rangle_{\beta\gamma}$ indicate that the integral sums over all unique permutations of β and γ. The cubic coupling constants are given by the overlaps

$$\begin{aligned} C^\alpha_{\beta\gamma\eta} = -T^{-1}\Big\langle &\Psi_\alpha^*(\sigma_{rr}[\Psi_\beta, \Psi_\gamma]\partial_\rho^2\Psi_\eta \\ &+ \mathrm{i}2n_\eta\sigma_{r\phi}[\Psi_\beta, \Psi_\gamma]\partial_\rho(\rho^{-1}\Psi_\eta) \\ &+ \sigma_{\phi\phi}[\Psi_\beta, \Psi_\gamma](\rho^{-1}\partial_\rho - n_\eta^2\rho^{-2})\Psi_\eta)\Big\rangle_{\beta\gamma\eta}. \end{aligned} \tag{23}$$

While equations (22) and (23) define the quadratic and cubic coupling constants one must, in order to explicitly evaluate them, know the mode functions Ψ_α. These are calculated in section 6 for arbitrary radius R and prestress T_0. The remaining unknown part of equation (20) is the eigenvalue Λ_α which are calculated in section 5 by means of perturbation theory.

5. Frequency spectrum

The frequency spectrum of the resonator is determined by $\hat{L}\Psi_\alpha + \Lambda_\alpha\Psi_\alpha = 0$. As the operator $\hat{V}$ is not uniform, the problem cannot, in general, be diagonalized analytically.

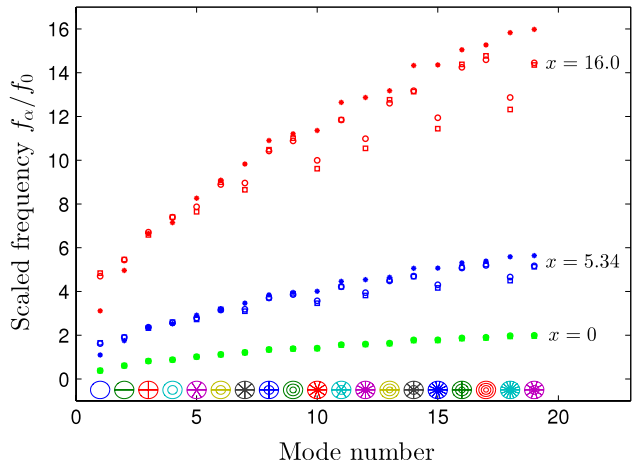

Figure 3. Frequency spectrum f_α on dimensionless form normalized with $f_0 = \sqrt{T_0/\rho_0 R^2}$, for arbitrary parameters R, T_0, ρ_0 and Eh. The 19 lowest lying flexural modes are plotted for three different values of $x = w_0 R^{-1}\sqrt{Eh(3-\nu)/T_0(1-\nu)}$. Green, blue and red symbols correspond to x equal to 0, 5.34 and 16.0. Circles: spectrum obtained using finite element simulations using $T_0 = 10^{-3}$ N m^{-1} and $R = 1$ μm. Squares: eigenfrequencies obtained using continuum theory incorporating deflection-induced non-uniform stress perturbatively to first order. Stars: eigenfrequencies obtained using only the uniform part of the deflection-induced stress. Note that the frequency crossings are not correctly reproduced unless the non-uniform part of the stress is included. Here, the Poisson ratio $\nu = 0.15$ was used.

Instead, we will use first order perturbation theory, treating the inhomogeneous part $\hat{V}$, defined in (21) as a perturbation. The unperturbed eigenfunctions are

$$\Psi^0_{n,k}(\rho,\phi) = \mathrm{e}^{\mathrm{i}n\phi} J_{|n|}(\lambda_{|n|,k}\,\rho)\Big/\sqrt{\pi}\,|J_{|n|+1}(\lambda_{|n|,k})| \quad (24)$$

for $n \in \mathbb{Z}$, $k \in \mathbb{N}$. Moreover, $J_n(x)$ is the nth Bessel function and $\lambda_{n,k}$ is the kth zero to the nth Bessel function. The first order correction to the spectrum is then $\Lambda^{(1)}_\alpha = \langle\Psi^0_\alpha \hat{V}\Psi^0_\alpha\rangle$ so that $\Lambda_\alpha \approx \Lambda^{(0)}_\alpha + \Lambda^{(1)}_\alpha$ with the unperturbed eigenvalues $\Lambda^{(0)}_\alpha = \lambda^2_\alpha$. Note that the stiffening due to the homogeneous part of the static stress is already present in the scaling of time. Hence, the perturbation only incorporates the inhomogeneous part of the stress.

Figure 3 shows the first order corrected frequencies $f_\alpha = \omega_\alpha/(2\pi) = \sqrt{(\Lambda^0_\alpha + \Lambda^1_\alpha)T/(\rho_0 R^2)}/(2\pi)$ under uniform load compared with the uncorrected prediction $f^0_\alpha = \omega^0_\alpha/(2\pi) = \sqrt{\Lambda^0_\alpha T/(\rho_0 R^2)}/(2\pi)$ along with COMSOL Multiphysics simulations including bending rigidity. Three different cases of the scaled static center deflection $x = w_0 R^{-1}\sqrt{Eh(3-\nu)/T_0(1-\nu)}$ are considered. For fixed prestress T_0 and material parameters Eh and ν, a stronger static voltage U_{dc} leads to a larger vertical deflection w_0 and therefore an increasing x. As can be seen, the first order corrections give a good estimate of the vibrational frequencies. A noteworthy result is that inclusion of the first order corrections leads to a decrease in frequency for modes with radial index $k = 1$. Whereas the frequencies increase monotonically with mode number for $x = 0$, for $x > 0$ non-monotonic behavior is seen, i.e. frequency crossings occur. This effect is not captured by the monotonically increasing uncorrected frequencies f^0_α.

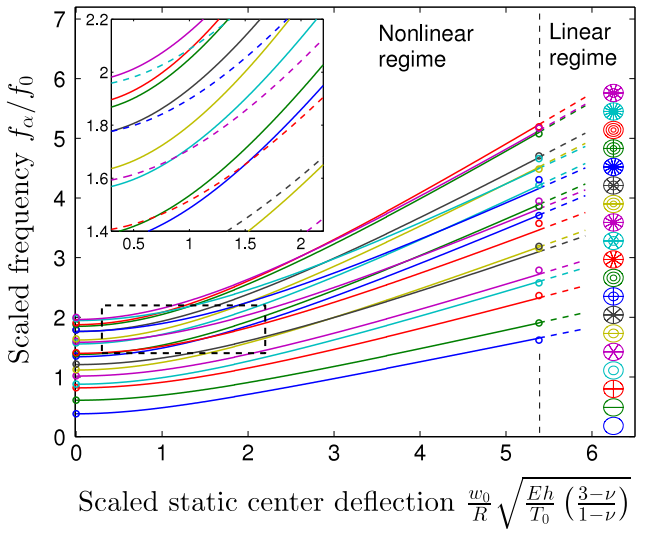

Figure 4. Frequency spectrum f_α on dimensionless form normalized with $f_0 = \sqrt{T_0/\rho_0 R^2}$ versus scaled static center deflection. The frequencies are color coded to their mode shapes on the right. (Solid lines) Spectrum from elasticity theory including first order perturbative corrections due to inhomogeneous stress. Circles: COMSOL Multiphysics simulations. The majority of frequency crossings of the higher frequencies are taking place in the range marked 'nonlinear regime'. In the region marked 'linear regime' the spectrum can be approximately obtained by linear extrapolation of the data in figure 3. The inset corresponds to the area in the rectangle and shows a zoomed in view of some of the frequency crossings. The dashed lines correspond to the frequencies with radial mode number $k = 1$. Here, the Poisson ratio $\nu = 0.15$ was used.

Figure 4 shows the region of parameter space where a majority of these frequency crossings occur. For large static deflections, $x \gtrsim 5.3$, frequencies approximately increase linearly with x and can therefore be extrapolated in this region from the data in figure 3.

If the load from the back-gate is modeled by (9) and expanded to the first order in $\delta\zeta$, electrostatic softening will shift the frequencies from

$$\begin{aligned} \omega^2_\alpha &\to \omega^2_\alpha - \omega^2_{\alpha,s}, \\ \omega^2_{\alpha,s} &\approx \varepsilon_0 U^2_{\mathrm{dc}} R/d^3 \rho_0 (1 + H_\alpha w_0/d + I_\alpha (w_0/d)^2), \end{aligned} \quad (25)$$

where H_α and I_α are numerical overlap integrals given in table 1. Introducing $\omega^0_\alpha = \lambda_\alpha R^{-1}\sqrt{T_0/\rho_0}$ the expressions for the frequencies take the form

$$\omega_\alpha = \omega^0_\alpha \sqrt{1 + x^2\,(1+\Gamma_\alpha)\,/4 - \left(\omega_{\alpha,s}/\omega^0_\alpha\right)^2}, \quad (26)$$

where Γ_α is given in table 1.

Defining $\Delta\omega_\alpha = \omega_\alpha - \omega^0_\alpha$ the total frequency tuning, including both stiffening due to deflection-induced tension as well as electrostatic softening, can thus be written as

$$\begin{aligned} \frac{\Delta\omega_\alpha}{\omega^0_\alpha} = &\left(1 + x^2\frac{(1+\Gamma_\alpha)}{4} - \frac{2}{\lambda^2_\alpha}\left(1 + H_\alpha\frac{w_0}{d} + I_\alpha\left(\frac{w_0}{d}\right)^2\right)\right. \\ &\left.\times\left(\frac{12 + x^2\left(\frac{7-\nu}{3-\nu}\right)}{3 - 8\frac{w_0}{d}}\right)\frac{w_0}{d}\right)^{1/2} - 1, \end{aligned} \quad (27)$$

where $x = w_0 R^{-1}\sqrt{EhT_0^{-1}(3-\nu)(1-\nu)^{-1}}$.

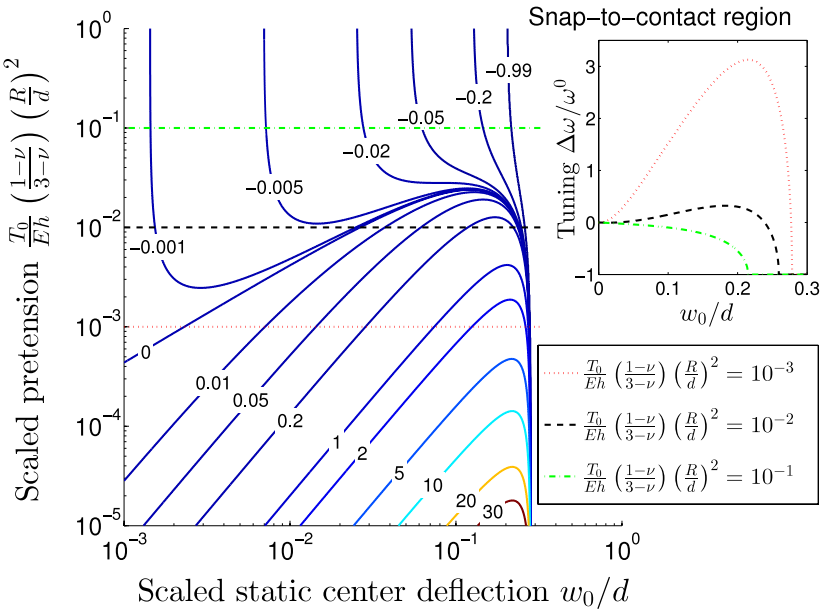

Figure 5. Frequency tuning of the fundamental mode including electrostatic softening according to equation (26). Solid lines: contours of constant relative frequency tuning $\Delta\omega/\omega^0$ of the fundamental flexural mode. Inset: the frequency tuning as a function of center deflection w_0/d for three different values of the product $(T_0/Eh)(R/d)^2$. The three curves correspond to the three horizontal lines (red dotted, black dashed and green dash-dotted) in the main figure. The region where snap-to-contact occurs is marked 'snap-to-contact region' and takes place for deflections in the range $0.2 < w_0/d < 0.3$. Here, the Poisson ratio $\nu = 0.15$ was used.

Table 1. Definitions of terms in equation (27) for the five lowest modes $\alpha = (n_\alpha, k_\alpha)$.

(n, k)	H_α	I_α	λ_α	$\Gamma_\alpha(3-\nu)$
(0, 1)	2.346	3.859	2.405	$(4.116 - 0.2892\nu)$
(1, 1)	2.000	2.873	3.832	$(2.046 + 0.1098\nu)\left(\frac{1+\nu}{3-\nu}\right)$
(2, 1)	1.773	2.290	5.136	$(-0.269 + 0.4577\nu)\left(\frac{1+\nu}{3-\nu}\right)$
(0, 2)	2.066	3.266	5.520	$(0.217 - 0.0791\nu)$
(3, 1)	1.607	1.902	6.380	$(-1.533 + 0.7171\nu)\left(\frac{1+\nu}{3-\nu}\right)$

The tuning of the fundamental mode is plotted in figure 5. For $(Eh)^{-1}T_0(3-\nu)^{-1}(1-\nu)R^2d^{-2} > 2.4 \times 10^{-2}$ the softening effect dominates for all deflections. With the typical values $R = 1\ \mu$m and $d = 300$ nm this corresponds to an initial tension of $T_0 = 2.5$ N m^{-1}, above which stiffening of the fundamental frequency is not observed. This is a very high tension compared with the values found in literature [2, 11].

The parallel plate approximation also predicts a snap-to-contact region for $0.2 < w_0/d < 0.3$ depending on x. Especially for low (scaled) prestress the tuning becomes larger with increasing (scaled) static center deflection and then drastically decreases and enters the snap-to-contact region.

6. Nonlinearities and mode coupling

We finally turn to the evaluation of the coefficients of the nonlinear terms in (1). Starting from (22) to (23), we note that by angular symmetry of the operators $\hat{L}$, $\hat{K}$ and the mode functions one finds

$$Q^\alpha_{\beta\gamma} \propto \delta_{n_\alpha, n_\beta + n_\gamma}, \qquad C^\alpha_{\beta\gamma\eta} \propto \delta_{n_\alpha, n_\beta + n_\gamma + n_\eta}, \tag{28}$$

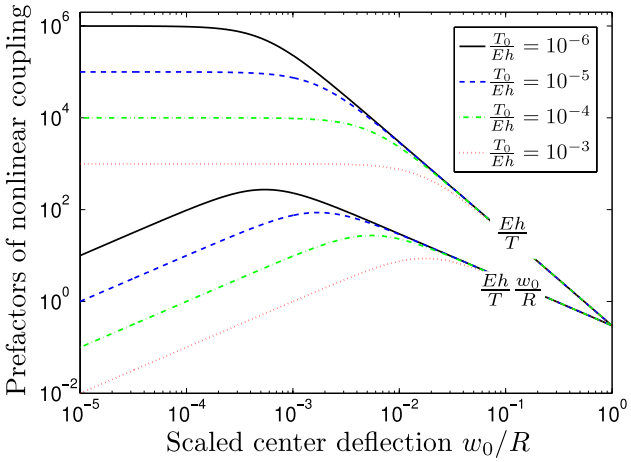

Figure 6. Prefactors of quadratic ($Q^\alpha_{\beta\gamma} \propto (Eh/T)[w_0/R]$) and cubic coupling constants ($C^\alpha_{\beta\gamma\eta} \propto Eh/T$) in equation (20) as functions of scaled static center deflection w_0/R.

where δ is the Kronecker-delta. The coupling constants take the form

$$Q^\alpha_{\beta\gamma} = \frac{Eh}{T}\frac{w_0}{R}\int_0^1 \mathrm{d}\rho\, K^\alpha_{\beta\gamma}(\rho, \nu),$$
$$Q^\alpha_{\beta\gamma\eta} = \frac{Eh}{T}\int_0^1 \mathrm{d}\rho\, K^\alpha_{\beta\gamma\eta}(\rho, \nu), \tag{29}$$

where $K^\alpha_{\beta\gamma}$ and $K^\alpha_{\beta\gamma\eta}$ correspond to the expressions in brackets (22) and (23). The prefactors are plotted in figure 6. The integrals depend on ν, but the dependences can be extracted analytically resulting in pure numerical integrals. By comparing with higher order corrections, we have found that it

Table 2. Cubic coupling constants between mode α equal 1–6 corresponding to mode indices $\alpha = (n_\alpha, k_\alpha)$ as $(0, 1)$, $(1, 1)$, $(-1, 1)$, $(2, 1)$, $(-2, 1)$ and $(0, 2)$, respectively. By symmetry, the tables for mode 3 and 5 are identical to the tables for mode 2 and 4 after interchanging $2 \leftrightarrow 3$ and $4 \leftrightarrow 5$. The constants are linearized according to $\Delta\nu = \nu - 0.15$.

$\beta\gamma\eta$	$\frac{T}{Eh} C^1_{\beta\gamma\eta}$	$\frac{T}{Eh} C^6_{\beta\gamma\eta}$	$\beta\gamma\eta$	$\frac{T}{Eh} C^2_{\beta\gamma\eta}$	$\beta\gamma\eta$	$\frac{T}{Eh} C^4_{\beta\gamma\eta}$
111	$3.92 + 3.68\Delta\nu$	-1.21	112	$12.5 + 7.95\Delta\nu$	114	$18.2 + 17.52\Delta\nu$
116	-3.63	$30.0 + 19.4\Delta\nu$	126	$-9.13 - 5.66\Delta\nu$	122	$13.2 - 4.76\Delta\nu$
123	$25.0 + 15.9\Delta\nu$	$-6.17 - 2.04\Delta\nu$	134	$29.8 - 16.7\Delta\nu$	146	$63.5 - 16.6\Delta\nu$
145	$35.0 + 38.3\Delta\nu$	$91.5 - 24.2\Delta\nu$	223	$69.0 + 44.2\Delta\nu$	226	$30.8 - 25.7\Delta\nu$
166	$30.0 + 19.4\Delta\nu$	-49.0	245	$121 + 59.6\Delta\nu$	234	$121 + 59.9\Delta\nu$
225	$0.509 - 5.57\Delta\nu$	$17.6 - 8.39\Delta\nu$	266	$57.5 + 45.9\Delta\nu$	445	$198 + 152\Delta\nu$
236	$-12.1 - 9.29\Delta\nu$	$115 + 91.8\Delta\nu$	346	$20.2 - 19.4\Delta\nu$	466	$271 + 22.0\Delta\nu$
334	$0.509 - 5.57\Delta\nu$	$17.6 - 8.39\Delta\nu$				
456	$22.5 + 9.88\Delta\nu$	$339 + 152\Delta\nu$				
666	-16.3	$172 + 102\Delta\nu$				

Table 3. Quadratic coupling constants between mode α equal 1 to 6 corresponding to mode indices $\alpha = (n_\alpha, k_\alpha)$ as $(0, 1)$, $(1, 1)$, $(-1, 1)$, $(2, 1)$, $(-2, 1)$ and $(0, 2)$, respectively. By symmetry, the tables for mode 3 and 5 are identical to the tables for mode 2 and 4 after interchanging $2 \leftrightarrow 3$ and $4 \leftrightarrow 5$. The constants are linearized according to $\Delta\nu = \nu - 0.15$.

$\beta\gamma$	$\frac{T}{Eh}\frac{R}{w_0} Q^1_{\beta\gamma}$	$\frac{T}{Eh}\frac{R}{w_0} Q^6_{\beta\gamma}$	$\beta\gamma$	$\frac{T}{Eh}\frac{R}{w_0} Q^2_{\beta\gamma}$	$\beta\gamma$	$\frac{T}{Eh}\frac{R}{w_0} Q^4_{\beta\gamma}$
11	$11.7 + 11.3\Delta\nu$	$-1.32 + 1.64\Delta\nu$	12	$26.8 + 18.5\Delta\nu$	14	$37.8 + 35.2\Delta\nu$
16	$-2.64 + 3.27\Delta\nu$	$54.4 + 39.6\Delta\nu$	26	$1.70 + 4.00\Delta\nu$	22	$21.4 + 4.37\Delta\nu$
23	$28.9 + 21.1\Delta\nu$	$6.41 + 9.75\Delta\nu$	34	$18.4 - 2.69\Delta\nu$	46	$45.7 + 22.3\Delta\nu$
45	$32.9 + 34.5\Delta\nu$	$44.0 + 22.0\Delta\nu$				
66	$27.2 + 19.8\Delta\nu$	$-11.4 + 25.9\Delta\nu$				

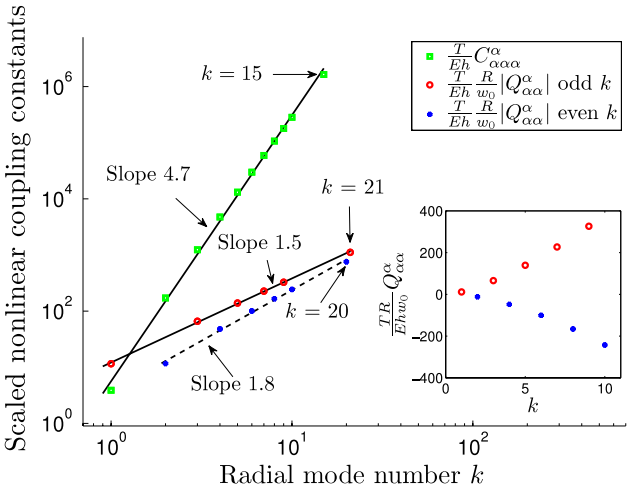

Figure 7. Diagonal quadratic and cubic coupling constants for symmetric modes, i.e., angular number $n = 0$. Here, the Poisson ratio $\nu = 0.15$ was used.

suffices to evaluate the integrals in (29) using the unperturbed mode functions Ψ^0_α defined in (24). The first order correction for the Duffing constant of the fundamental mode reduces it with 6% in the worst case scenario. The Duffing constants $C^\alpha_{\alpha\alpha\alpha}$ for the symmetric modes are plotted in figure 7 showing power-law behavior with a small curvature correction.

The cubic and quadratic coupling constants for the 6 lowest lying flexural modes are tabulated in tables 2 and 3, respectively. They have been linearized around $\nu = 0.15$ and for small deviations from this value, $\Delta\nu = \nu - 0.15$ can to a good approximation be set to zero except for the coupling constants C^1_{225} and C^1_{334}.

7. Conclusions

Based on a continuum mechanical formulation, we have derived the nonlinear coupled equations of motion for a circular membrane resonator and analyzed both the eigenfrequency spectrum as well as the nonlinear coefficients entering the equations of motion for the mode amplitudes. For the static mode shape, due to the dc component of the bias, we find that a simple algebraic Ansatz compares well with finite element simulations for realistic device parameter values. For the eigenfrequency spectrum we further find that it suffices to incorporate the first order perturbative corrections to reproduce both qualitatively and quantitatively the spectrum for the lowest lying modes. In particular, we find that only by incorporating the inhomogeneous part of the deflection-induced stress will one correctly reproduce frequency crossings which occur with increasing static bias voltage. We have further derived expressions for the nonlinear coefficients, quadratic and cubic, which must be taken into account when modeling the dynamic response of ultrathin NEM-resonators.

Acknowledgments

The authors acknowledge funding from the European union (ME, DM, AI) through FP7 project no. 246026 (RODIN) and the Swedish Research Council VR (AC, AI).

Appendix. Solving the Airy stress equation

To find the in-plane stresses we need to solve an inhomogeneous biharmonic equation of the form $\Delta^2\chi(\rho, \phi) = f(\rho, \phi)$

on the unit disk $0 < \rho < 1, 0 \leq \phi < 2\pi$. Periodicity in ϕ implies that we can Fourier expand χ and f as $\chi = \sum_n e^{in\phi}\chi_n(\rho)$ and $f = \sum_n e^{in\phi} f_n(\rho)$ leaving us with the problem $\Delta_n^2\chi_n = f_n(\rho)$, where $\Delta_n\chi_n \equiv \rho^{|n|-1}\partial_\rho\left(\rho^{1-2|n|}\partial_\rho\rho^{|n|}\chi_n\right)$. Repeated integration over ρ shows that the general solutions can be expressed as $\chi_n(\rho) = \chi_n^{(p)}(\rho) + H_{|n|}(\rho)$, where

$$\chi_n^{(p)}(\rho) = \rho^2 \int_0^\rho \mathrm{d}\rho\, G_{|n|}(\rho/\rho')\rho' f(\rho'),$$

with the Kernels $G_0(\xi) = \frac{1}{4}([\xi^{-2} + 1]\ln\xi + \xi^{-2} - 1)$, $G_1(\xi) = \frac{1}{16\xi}[\xi^2 - \xi^{-2} - 4\ln\xi]$ and $G_{n\geq 2}(\xi) = \frac{1}{8n}(\frac{1}{n+1}[\xi^n - \xi^{-n-2}] + \frac{1}{n-1}[\xi^{-n} - \xi^{n-2}])$. The terms $H_n(\rho)$ contain the nonsingular homogeneous solutions $H_0 = A_0\rho^2$, $H_1 = A_1\rho^3$, and $H_{n\geq 2} = A_n\rho^{n+2} + B_n\rho^n$. The constants A_n, B_n are chosen such that the in-plane displacement fields satisfy the boundary conditions (8), resulting in

$$\begin{aligned}
A_0 &= -2^{-1}(1-\nu)^{-1}(\partial_\rho^2 - \nu\partial_\rho)\chi_0^{(p)}|_{\rho=1},\\
A_1 &= -2^{-1}(3-\nu)^{-1}(\partial_\rho^2 - \nu[\partial_\rho - 1])\chi_1^{(p)}|_{\rho=1},\\
A_n &= -(4n)^{-1}(3-\nu)^{-1}(2I_1(1) + (n-1)[I_2(1) + 2I_3(1)]),\\
B_n &= -\{[n(1+\nu) - 2(1-\nu)]2I_1(1)\\
&\quad + (n+1)[n(1+\nu) + 2(1-\nu)][I_2(1) + 2I_3(1)]\}\\
&\quad \times [4n^2(3-\nu)(1+\nu)]^{-1},
\end{aligned}$$

where

$$\begin{aligned}
I_1(x) &= (\partial_x^2 - \nu[\partial_x - n^2])\chi_n^{(p)},\\
I_2(x) &= \int_0^x \mathrm{d}x'\ (\partial_{x'}\zeta(x'))^2,\\
I_3 &= \nu\partial_x\chi_n^{(p)} - \int_0^x \mathrm{d}x'(x'^{-1}\partial_{x'} - n^2x'^{-2})\chi_n^{(p)}.
\end{aligned}$$

For the particular problem in this paper, we need to solve a stress problem on the form $\Delta^2\chi = F[\zeta,\zeta]$ where F is the bilinear operator on the vertical displacement field ζ,

$$\begin{aligned}
F[\zeta,\zeta'] = &-\tfrac{1}{2}(\partial_\rho\zeta)(\rho^{-1}\partial_\rho\zeta' + \rho^{-2}\partial_\phi^2\zeta')\\
&-\tfrac{1}{2}(\rho^{-1}\partial_\rho\zeta + \rho^{-2}\partial_\phi^2\zeta)(\partial_\rho^2\zeta')\\
&+\partial_\rho\rho^{-1}\partial_\phi\zeta(\partial_\rho\rho^{-1}\partial_\phi\zeta').
\end{aligned}$$

Writing $\zeta = \bar{\zeta} + \sum_\alpha\zeta_\alpha\Psi_\alpha$ and using the bilinearity of F one finds

$$\begin{aligned}
\Delta^2\chi &= F\left[\bar{\zeta} + \sum_\alpha\zeta_\alpha\Psi_\alpha, \bar{\zeta} + \sum_\beta\zeta_\beta\Psi_\beta\right]\\
&= F[\bar{\zeta},\bar{\zeta}] + 2\sum_\alpha\zeta_\alpha F[\bar{\zeta},\Psi_\alpha] + \sum_{\alpha,\beta}\zeta_\alpha\zeta_\beta F[\Psi_\alpha,\Psi_\beta].
\end{aligned}$$

Linearity of Δ^2 allows us to write the solution as $\chi = \bar{\chi} + 2\sum_\alpha\zeta_\alpha\chi^\alpha + \sum_{\alpha\beta}\zeta_\alpha\zeta_\beta\chi^{\alpha,\beta}$, where the terms satisfy individually the equations $\Delta^2\bar{\chi} = F[\bar{\zeta},\bar{\zeta}]$, $\Delta^2\chi^{(\alpha)} = F[\bar{\zeta},\Psi_\alpha]$, $\Delta^2\chi^{(\alpha,\beta)} = F[\Psi_\alpha,\Psi_\beta]$. Solution by Fourier expansion and integration as above is now possible and we find (using $\bar{\zeta} = \zeta_0(1-\rho^2)$)

$$\begin{aligned}
\bar{\chi} &= \bar{\chi}_0 = -\tfrac{1}{16}\zeta_0^2\rho^4 + \bar{H}_0,\\
\chi_n^\alpha &= \zeta_0\rho\int_0^\rho \mathrm{d}\rho'\,\Psi_\alpha(\rho')K_{|n|}(\rho/\rho') + H_{|n|}^{(\alpha)},\\
\chi_n^{\alpha,\beta} &= \rho^2\int_0^\rho \mathrm{d}\rho'\,F_n[\Psi_\alpha(\rho'),\Psi_\beta(\rho')]\rho' G_{|n|}(\rho/\rho') + H_{|n|}^{(\alpha,\beta)},
\end{aligned}$$

with the new additional kernels $K_0(\xi) = \xi^{-1}\ln\xi$, $K_1(\xi) = \frac{1}{2}[1 - \xi^{-2}]$, and $K_{n\geq 2} = \frac{1}{2n}[\xi^{n-1} - \xi^{-n-1}]$. The stress components are then given by the derivatives (12).

References

[1] Karabalin R B, Cross M C and Roukes M L 2009 *Phys. Rev.* B **79** 165309
[2] Eichler A, Moser J, Chaste J, Zdrojek M, Wilson-Rae I and Bachtold A 2011 *Nature Nanotechnol.* **6** 339
[3] Eichler A, Ruiz M D, Plaza J A and Bachtold A 2012 *Phys. Rev. Lett.* **109** 025503
[4] Matheny M H, Villanueva L G, Karabalin R B, Sader J E and Roukes M L 2013 *Nano Lett.* **13** 1622
[5] Faust T, Rieger J, Seitner M J, Kotthaus J P and Weig E M 2013 *Nature Phys.* **9** 485
[6] Mahboob I, Nishiguchi K, Fujiwara A and Yamaguchi H 2013 *Phys. Rev. Lett.* **110** 127202
[7] Okamoto H, Gourgout A, Chang C-Y, Onomitsu K, Mahboob I, Chang E Y and Yamaguchi H 2012 arXiv:1212.3097
[8] Westra H J R, Poot M, van der Zant H S J and Venstra W J 2010 *Phys. Rev. Lett.* **105** 117205
[9] Venstra W J, van Leeuwen R and van der Zant H S J 2012 *Appl. Phys. Lett.* **101** 243111
[10] Zaitsev S, Shtempluck O, Buks E and Gottlieb O 2012 *Nonlinear Dyn.* **67** 859
[11] Bunch J S, van der Zande A M, Verbridge S S, Scott S, Frank I W, Tanenbaum D M, Parpia J M, Craighead H G and McEuen P L 2007 *Science* **315** 490
[12] Barton R A, Ilic B, van der Zande A M, Whitney W S, McEuen P L, Parpia J M, Jeevak M and Craighead H G 2011 *Nano Lett.* **11** 1232
[13] Song X, Oksanen M, Sillanpää M A, Craighead H G, Parpia J M and Hakonen P J 2012 *Nano Lett.* **12** 198
[14] Chen C Y, Rosenblatt S, Bolotin K I, Kalb W, Kim P, Kymissis I, Stormer H L, Heinz T F and Hone J 2009 *Nature Nanotechnol.* **4** 861
[15] Xu Y H, Chen C Y, Deshpande V V, DiRenno F A, Gondarenko A, Heinz D B, Liu S M, Kim P and Hone J 2010 *Appl. Phys. Lett.* **97** 243111
[16] Singh V, Sengupta S, Solanki H S, Dhall R, Allain A, Dhara S, Pant P and Deshmukh M M 2010 *Nanotechnology* **21** 165204
[17] Singh V, Irfan B, Subramanian G, Solanki H S, Sengupta S, Dubey S, Kumar A, Ramakrishnan S and Deshmukh M M 2012 *Appl. Phys. Lett.* **100** 233103
[18] Zhou Q and Zettl A 2013 *Appl. Phys. Lett.* **102** 223109
[19] Atalaya J, Isacsson A and Kinaret J M 2008 *Nano Lett.* **8** 4196
[20] Croy A, Midtvedt D, Isacsson A and Kinaret J M 2012 *Phys. Rev.* B **86** 235435
[21] Ruiz-Vargas C S, Zhuang H L, Huang P Y, van der Zande A M, Garg S, McEuen P L, Muller D A, Hennig R G and Park J 2011 *Nano Lett.* **11** 2259
[22] Liu J, Usami K, Naesby A, Bagci T, Polzik E S, Lodahl P and Stobbe S 2011 *Appl. Phys. Lett.* **99** 243102
[23] Adiga V P, Ilic B, Barton R A, Wilson-Rae I, Craighead H G and Parpia J M 2012 *J. Appl. Phys.* **112** 064323
[24] Atalaya J, Kinaret J M and Isacsson A 2010 *Europhys. Lett.* **91** 48001
[25] Voje A, Kinaret J M and Isacsson A 2012 *Phys. Rev.* B **85** 205415
[26] Voje A, Croy A and Isacsson A 2013 *New J. Phys.* **15** 053041

[27] Garcia-Sanchez D, van der Zande A M, San Paulo A, Lassagne B, McEuen P L and Bachtold A 2008 *Nano Lett.* **8** 1399
[28] Kim S Y and Park H S 2009 *Nano Lett.* **9** 969
[29] Robinson J T, Zalalutdinov M, Baldwin J W, Snow E S, Wei Z, Sheehan P and Houston B H 2008 *Nano Lett.* **8** 3441
[30] Katsnelson M I and Fasolino A 2013 *Acc. Chem. Res.* **46** 97
[31] Hencky H 1915 *Z. Math. Phys.* **63** 311
[32] Dickey R W 1967 *Arch. Ration. Mech. Anal.* **26** 219
[33] Yen D H Y and Lee T W 1975 *Int. J. Nonlinear Mech.* **10** 47
[34] Jenkins C H 1996 *Appl. Mech. Rev.* **49** S41
[35] Kudin K N, Scuseria G E and Yakobson B I 2001 *Phys. Rev.* B **64** 235406
[36] Lindahl N, Midtvedt D, Svensson J, Nerushev O A, Lindvall N, Isacsson A and Campbell E E B 2012 *Nano Lett.* **12** 3526
[37] Roldán R, Fasolino A, Zakharchenko K V and Katsnelson M I 2011 *Phys. Rev.* B **83** 174104
[38] Timoshenko S P and Woinowsky-Krieger S 1959 *Theory of Plates and Shells* 2nd edn (London: McGraw-Hill)
[39] Landau L D and Lifshitz E M 1986 *Theory of Elasticity* 3rd edn (New York: Elsevier)
[40] Fasolino A, Los J H and Katsnelson M I 2007 *Nature Mater.* **6** 858
[41] Bao W, Miao F, Chen Z, Zhang H, Jang W, Dames C and Lau C N 2009 *Nature Nanotechnol.* **4** 861